J. Fluid Mech. (2011), *vol.* 688, *pp.* 507–527.
doi:10.1017/jfm.2011.398

Rayleigh–Taylor mixing in an otherwise stable stratification

Andrew G. W. Lawrie† and Stuart B. Dalziel

Department of Applied Mathematics and Theoretical Physics, University of Cambridge, Wilberforce Road, Cambridge CB3 0WA, UK

(Received 30 July 2010; revised 17 May 2011; accepted 15 September 2011; first published online 3 November 2011)

We seek to understand the distribution of irreversible energy conversions (mixing efficiency) between quiescent initial and final states in a miscible Rayleigh–Taylor driven system. The configuration we examine is a Rayleigh–Taylor unstable interface sitting between stably stratified layers with linear density profiles above and below. Our experiments in brine solution measure vertical profiles of density before and after the unstable interface is allowed to relax to a stable state. Our analysis suggests that less than half the initially available energy is irreversibly released as heat due to viscous dissipation, while more than half irreversibly changes the probability density function of the density field by scalar diffusion and therefore remains as potential energy, but in a less useful form. While similar distributions are observed in Rayleigh–Taylor driven mixing flows between homogeneous layers, our new configuration admits energetically consistent end-state density profiles that span all possible mixing efficiencies, ranging from all available energy being expended as dissipation, to none. We present experiments that show that the fluid relaxes to a state with a significantly lower mixing efficiency than the value for ideal mixing in this configuration, and deduce that this mixing efficiency more accurately characterizes Rayleigh–Taylor driven mixing than previous measurements. We argue that the physical mechanisms intrinsic to Rayleigh–Taylor instability are optimal conditions for mixing, and speculate that we have observed an upper bound to fluid mixing in general.

Key words: buoyancy-driven instability, stratified turbulence, turbulent mixing

1. Introduction

Understanding turbulent transport and energy conversion processes in stratified fluids is an ongoing scientific challenge, and the implications of such processes reach well beyond the confines of science. To take but one example, scalar transport – of both temperature and salt – is fundamental to oceanic circulation, and fluctuations therein strongly influence our climate. Our focus here is on how molecular-scale processes in turbulent fluid systems, the intricate details of which are of interest only to specialist communities, influence on a measurable scale the aggregate behaviour of quantities that are of widespread interest. In particular, we examine how molecular mixing influences the transport of advected scalars and the conversion of energy.

Mixing between two species is a two-step process that comprises stirring and molecular diffusion. Molecular diffusion alone is a slow process and the stirring

† Email address for correspondence: A.G.W.Lawrie@damtp.cam.ac.uk

enhances the rate of species diffusion by stretching material surfaces and increasing the surface area and the species gradient over which the molecular diffusion occurs. Rayleigh–Taylor unstable flows are especially interesting to examine in this context because, throughout the evolution of the instability, the baroclinic source term in the vorticity equation, $-(1/\rho^2)\nabla\rho \times \nabla p$, deposits vorticity into the flow oriented perpendicular to, and precisely co-located with, the species/scalar gradients. Since gradients of the induced velocity decay exponentially away from the vorticity source, co-location and perpendicular orientation are the optimal conditions for the sustained stretching of material surfaces. One would expect from this that Rayleigh–Taylor instability is unusually effective at doing mixing, and indeed this has been shown to be the case (e.g. Linden, Redondo & Youngs 1994; Dalziel *et al.* 2008).

The classical Rayleigh–Taylor problem can be characterized very simply by the following unstable initial condition:

$$\rho(z) = \begin{cases} \rho_u, & z \geqslant 0, \\ \rho_l, & z < 0, \end{cases} \tag{1.1}$$

where $\rho_u > \rho_l$ are constant densities and z is anti-parallel to the acceleration field, which in the laboratory context is gravity, g. In the absence of surface tension, any perturbation to the interface will initiate a self-perpetuating, internally driven flow, which becomes turbulent at sufficiently high Re. Potential energy is released into kinetic energy by local overturning of dense and light fluid, which expands the mixing region at the expense of the unmixed regions. Some of that kinetic energy is used to engulf further unmixed fluid and this accelerates the instability. The rate at which this process happens (in the high Re regime) is controlled by the acceleration due to reduced gravity, $g' = g(\Delta\rho/\overline{\rho})$, where in this classic Rayleigh–Taylor context we have $\Delta\rho = \rho_u - \rho_l$ and for Boussinesq density differences, $\overline{\rho} = (\rho_u + \rho_l)/2$. In the majority of the Rayleigh–Taylor literature, a non-dimensional density difference is introduced, the Atwood number,

$$A = \frac{\rho_u - \rho_l}{\rho_u + \rho_l}, \tag{1.2}$$

and is related to the reduced gravity by $g' = 2Ag$. On dimensional grounds alone, the height h of the mixing region must be characterized by $h \sim f(A)gt^2$, and there is a wealth of evidence to suggest that $f(A) = A$ both for Boussinesq flows and for the penetration of light into dense for non-Boussinesq flows. It is common to write an expression for the instability growth in the form $h = \alpha Agt^2$, where by convention the constant of proportionality is denoted α. Defining its value has attracted much experimental (e.g. Read 1984; Snider & Andrews 1994; Dalziel, Linden & Youngs 1999; Waddell, Niederhaus & Jacobs 2001), numerical (e.g. Youngs 1984; Cook, Cabot & Miller 2004; Dimonte *et al.* 2004; Cabot & Cook 2006) and modelling (e.g. Zufiria 1988; Ofer *et al.* 1996; Rikanati *et al.* 2000) interest over the past 25 years, yet many uncertainties remain.

It is reasonable to infer that the rate of instability growth is controlled by the distribution of energy in the system, particularly the balance between energy needed to sustain the instability and energy used in other ways. We have chosen to look at Rayleigh–Taylor unstable systems from this perspective, and we measure experimentally the energetic changes between initial and final states. Experimentally this poses problems for an unconfined instability (which will evolve *ad infinitum*), unless one accepts the somewhat arbitrary confinement imposed by a finite domain.

We consider instead a case where the Rayleigh–Taylor instability is naturally confined by linear stable density stratifications that sit above and below the Rayleigh–Taylor unstable interface. The stratification at $t = 0$ is given by

$$\rho(z, 0) = \begin{cases} \rho_u - \beta z, & z \geqslant 0, \\ \rho_l - \beta z, & z < 0, \end{cases} \tag{1.3}$$

where the constant stratification slope β is given by

$$\beta = -\frac{\partial \rho}{\partial z} = \frac{\overline{\rho}}{g} N^2 > 0. \tag{1.4}$$

Here, N is the buoyancy frequency and $\rho_u > \rho_l$ are the densities just above and below the interface. The initial density field $\rho(z, 0)$ is of course discontinuous and Rayleigh–Taylor unstable at $z = 0$. In the case $\beta = 0$, equation (1.3) reduces to the classic Rayleigh–Taylor problem.

The decomposition of energy into kinetic and potential components is elementary, but in characterizing the energy conversions here we follow Winters *et al.* (1995) and decompose potential energy into 'available' and 'background' components. Potential energy has a component 'available' (in a thermodynamic sense) to do work, E_{ap}, and a remainder component known as the 'background', E_{bp}, which has no capacity to do further work. All kinetic energy, E_k, currently in the system is considered available, so E_a, the energy available to the system for conversion to another form, is given by $E_a = E_k + E_{ap}$. As the system relaxes, progressively less of this energy will remain available. Ultimately, a quiescent, stable state is reached.

The question this paper examines is where that initially available energy ends up. For more complex and larger systems, one must take into account conversion to and from chemical potential energy and other higher-order concerns (see Tailleux 2009, for a detailed discussion), but here our data are taken at laboratory scale and concern the behaviour of miscible liquids under linear mixing at atmospheric pressure. With these restrictions, we can construct a Boussinesq, incompressible model, accounting for contributions to internal energy E_i but ignoring any feedback from it. Such effects we thus neglect include the very long time scale processes of diffusion that occur in the absence of stirring (see Winters & Young 2009, for some details), heat-induced volumetric expansion and contributions from dissolution due to diffusion of our density-varying solute, sodium chloride. These assumptions can be shown to introduce errors two orders of magnitude smaller than those experimental errors we are able to measure, and so we choose to ignore such effects. However, even the weak nonlinearities of the equation of state for sea water are likely to become important at oceanographic scales.

At a continuum scale, we regard shear as the physical mechanism by which kinetic energy is converted to heat, and viscosity ν controls the rate at which this happens. Less intuitively, molecular diffusion of mass, controlled by a scalar diffusivity κ, is the corresponding mechanism by which available potential energy E_{ap} is converted to background potential energy E_{bp}. This mechanism can perhaps best be described by considering how mixing changes the form of the density field probability density function (p.d.f.(ρ)). In general, mixing takes a pre-existing contrast in density and afterwards fluid is concentrated closer to some mean density. There is an irreversible energy conversion associated with this process, which one could quantify if one were to associate the p.d.f. with a unique monotonic stable stratification. The sorting of the density field required to obtain a p.d.f. (see Tseng & Ferziger 2001) is equivalent to

that required to adiabatically rearrange arbitrarily located fluid parcels into a stable state, i.e. $sort(\rho(\boldsymbol{x})) = \rho(\hat{z})$, where $\hat{z}$ is the required vertical reorganization. When density contrasts are eroded by mixing towards a mean density, the centre of mass of the reorganized field is lifted upwards, so the corresponding integral 'background' potential energy, $E_{bp} = \int_V \rho g \hat{z}\, \mathrm{d}V$, therefore increases over time.

With the above arguments, we can thus identify that there are two primary routes for initially available energy to become unavailable, namely a flux to internal energy and a flux to background potential energy. These can most simply be described by the following differential system for the aggregate energy:

$$\frac{\mathrm{d}E_i}{\mathrm{d}t} = \epsilon, \tag{1.5a}$$

$$\frac{\mathrm{d}E_k}{\mathrm{d}t} = -\phi - \epsilon, \tag{1.5b}$$

$$\frac{\mathrm{d}E_{ap}}{\mathrm{d}t} = \phi - \zeta, \tag{1.5c}$$

$$\frac{\mathrm{d}E_{bp}}{\mathrm{d}t} = \zeta, \tag{1.5d}$$

where the energy conversion fluxes follow from the Boussinesq equations of motion (see Winters *et al.* 1995, for more detail) and reduce to:

$$\epsilon(t) = \int_V \nu |\boldsymbol{\nabla u}|^2 \, \mathrm{d}V, \tag{1.6a}$$

$$\zeta(t) = -\kappa g \int_V \frac{\mathrm{d}\hat{z}}{\mathrm{d}\rho} |\boldsymbol{\nabla}\rho|^2 \, \mathrm{d}V, \tag{1.6b}$$

$$\phi(t) = \int_V g \rho \boldsymbol{u}_z \, \mathrm{d}V. \tag{1.6c}$$

The dissipative flux, $\epsilon(t) \geqslant 0$, is the flux to internal energy due to friction; $\zeta(t) \geqslant 0$ is the flux of energy to background, which we note is a non-local definition, since it requires knowledge of the complete system to obtain $\hat{z}$. Both are non-negative and irreversible due to processes on the molecular scale. The buoyancy flux $\phi(t)$, which represents the work done on the density field by the velocity field, is an adiabatic, reversible exchange between the two forms of available energy.

The fluxes ζ and ϵ together quantify the rate of decrease of available energy, but it is of interest to examine the distribution of energy leaving the system, in particular the ratio ζ/ϵ, first used by Oakey (1982). A commonly used alternative, especially in the oceanographic community (e.g. Itsweire *et al.* 1992; Munk & Wunsch 1998; Wunsch & Ferrari 2004; Laurent, Simmons & Jayne 2006), is the mixing efficiency η. In our current framework we define the instantaneous mixing efficiency as

$$\eta_I = \frac{\zeta}{\zeta + \epsilon}. \tag{1.7}$$

Rayleigh–Taylor instability is unusual for its quiescent initial and final states, and in a laboratory context it is very convenient to measure changes in aggregate quantity between end states in a closed system. We adopt the definition for an 'aggregate'

mixing efficiency

$$\eta_A = \frac{|\Delta E_{bp}|}{|\Delta E_{ap} + \Delta E_k|}, \tag{1.8}$$

and for convenience use absolute values, since $\Delta E_a = \Delta E_{ap} + \Delta E_k < 0$ and $\Delta E_{bp} > 0$. In the special case of Rayleigh–Taylor instability, which has quiescent initial and end states, $\Delta E_k = 0$ and $\Delta E_a = \Delta E_{ap}$.

We now consider how aggregate mixing efficiency in the classical Rayleigh–Taylor case can be predicted from the initial density profile and assumptions about the expected final state. As shown in figure 1(*a*), the initial state has a p.d.f. given by $\delta(\rho - \rho_u) + \delta(\rho - \rho_l)$ (where δ is the Dirac delta function). If we assume that the most mixing possible has taken place by the time the flow comes to rest, then the end state would be homogeneous at the mean density, and we would have a density field p.d.f. given by $2\delta[\rho - (\rho_u + \rho_l)/2]$. Experimentally we get remarkably close to this (see Holford, Dalziel & Youngs 2003) in low-aspect-ratio domains (though variability in initial conditions has a small influence), and even closer in high-aspect-ratio domains (see Dalziel *et al.* 2008), where the initial conditions have negligible influence.

With this empirically supported model for the evolution of the p.d.f., we obtain corresponding potential energies:

$$E^0_{tp} = \int_{-H}^{0} \rho_l g z \,\mathrm{d}z + \int_{0}^{H} \rho_u g z \,\mathrm{d}z = \frac{1}{2} g H^2 (\rho_u - \rho_l), \tag{1.9a}$$

$$E^0_{bp} = \int_{-H}^{0} \rho_u g z \,\mathrm{d}z + \int_{0}^{H} \rho_l g z \,\mathrm{d}z = \frac{1}{2} g H^2 (\rho_l - \rho_u) = -E^0_{tp}, \tag{1.9b}$$

$$E^\infty_{bp} = \int_{-H}^{H} \frac{\rho_u + \rho_l}{2} g z \,\mathrm{d}z = 0, \tag{1.9c}$$

$$E^\infty_{tp} = E^\infty_{bp}, \tag{1.9d}$$

where the *tp* suffix we introduce here indicates the total potential energy. With our current definition of $z = 0$, the background potential energy at the end state, E^∞_{bp}, cannot be greater than zero, even if the stratification is not well mixed. The maximum mixing efficiency, in terms of these total and background potential energies, is given by

$$\eta_A|_{max} = \frac{|E^\infty_{bp} - E^0_{bp}|}{|(E^\infty_{tp} - E^\infty_{bp}) - (E^0_{tp} - E^0_{bp})|} = \frac{1}{2}. \tag{1.10}$$

This result is well known for the classic Rayleigh–Taylor problem in a finite box, and indeed no closed process has been shown to exhibit higher mixing efficiencies than Rayleigh–Taylor instability. Furthermore, it is straightforward to show that $\eta_A|_{max} = 1/2$ holds for any monotonic density profile anti-symmetric about its mid-point, of the form

$$\rho(z, 0) = \begin{cases} \overline{\rho} + \Delta\rho(|z|), & z > 0, \\ \overline{\rho} - \Delta\rho(|z|), & z < 0. \end{cases} \tag{1.11}$$

As for the classical instability, $E^0_{bp} = -E^0_{tp}$ and $E^\infty_{bp} = 0 = E^\infty_{tp}$ for a well-mixed final state. However, we have not been able to verify our prediction experimentally, since we cannot generate unstable stratifications of this form in the present experimental

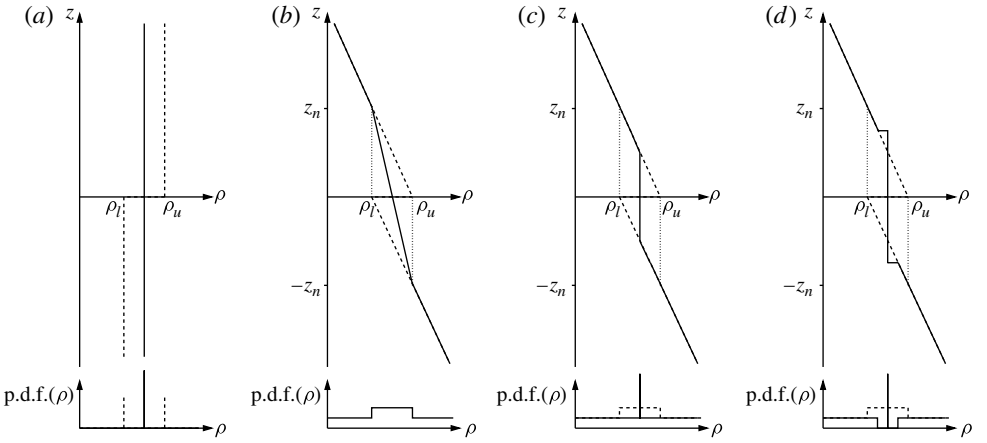

FIGURE 1. Idealized stratifications and probability density functions of initial and final states for (*a*) the classical Rayleigh–Taylor instability, and (*b–d*) the new stratified configuration under the limiting conditions of (*b*) no mixing, (*c*) 'complete' mixing and (*d*) no dissipation. Initial states are shown as dashed lines, and final states as solid lines.

apparatus. The significance of this prediction, however, is that the end state will approach a well-mixed state for any monotonically unstable initial stratification, irrespective of the initially available potential energy. In this sense, such initial density profiles possess *excess* available energy that can only be expended by doing additional dissipation beyond the minimum needed to perform the mixing that achieves a well-mixed end state. Observation of their final quiescent states therefore indicates little about the the minimum dissipation needed to perform mixing specifically during the Rayleigh–Taylor mixing process. The key question is obvious: what might we learn if we remove the 'excess' energy?

We now turn our attention to the system described by (1.3). It is not clear *a priori* what the end-state profile will be, but, as illustrated by the sequence of figure 1(*b–d*), we can construct well-defined bounds. Once again it is instructive to consider both the p.d.f. of the density field, and its mean vertical profile.

If all fluid parcels were mutually immiscible, no mixing could take place between them, so the p.d.f. would remain unchanged throughout the process, and therefore the background state that we define from the sorting would also remain unchanged. Therefore, once all available energy was used, the final state would have been identical to the initial background state. Since no energy was spent modifying the background state, all the irreversible energy conversions must have been dissipative (i.e. $\eta_A = 0$) and the system relaxation must simply have been a rearrangement of fluid parcels without modification of their properties. This final state is illustrated in figure 1(*b*), and we note that the mixing region must penetrate vertically until those fluid parcels that are initially most buoyant reach a position where they become neutrally buoyant. We denote this point

$$z_n = \frac{\rho_u - \rho_l}{\beta}, \tag{1.12}$$

as indicated in the figure.

Now consider the case conceptually closest to perfect mixing, where there is sufficient advective transport within the mixing region that every newly encountered

fluid parcel of density ρ at the upper edge of the mixing region can pair and mix with its equal and opposite member $2\overline{\rho}-\rho$ on the lower edge and thus generate fluid of density $\overline{\rho}=(\rho_u+\rho_l)/2$. The p.d.f., initially distributed as a top-hat profile, will become narrower from the outside and eventually become a Dirac delta function. The mixed region will be homogeneous, with density $\overline{\rho}$, and its vertical penetration, by geometric reasoning, can be no further than $\pm z_n/2$, as shown in figure 1(*c*). We calculate the energy conversions that give rise to this end state as

$$E_{tp}^{0}=\int_{-z_n}^{0}(\rho_l-\beta z)\,gz\,\mathrm{d}z+\int_{0}^{z_n}(\rho_u-\beta z)\,gz\,\mathrm{d}z$$
$$=-\frac{1}{6}(\rho_u-\rho_l)\,gz_n^2, \tag{1.13a}$$
$$E_{bp}^{0}=\int_{-z_n}^{z_n}\left(\frac{\rho_u+\rho_l}{2}-\frac{\rho_u-\rho_l}{2z_n}z\right)gz\,\mathrm{d}z$$
$$=-\frac{1}{3}(\rho_u-\rho_l)\,gz_n^2, \tag{1.13b}$$
$$E_{tp}^{\infty}=\int_{-z_n}^{-z_n/2}(\rho_l-\beta z)\,gz\,\mathrm{d}z+\int_{-z_n/2}^{z_n/2}\frac{\rho_u+\rho_l}{2}gz\,\mathrm{d}z+\int_{z_n/2}^{z_n}(\rho_u-\beta z)\,gz\,\mathrm{d}z$$
$$=-\frac{5}{24}(\rho_u-\rho_l)\,gz_n^2, \tag{1.13c}$$
$$E_{bp}^{\infty}=E_{tp}^{\infty}. \tag{1.13d}$$

This results in an aggregate mixing efficiency of

$$\eta_A=\tfrac{3}{4}. \tag{1.14}$$

Note that the vertical penetration of the mixing region is smaller for $\eta_A=3/4$ than for $\eta_A=0$. This raises the question of how one could obtain $\eta_A=1$, which would represent an inviscid fluid with no dissipation. In this case all irreversible energy conversions must be due to molecular diffusion of density. We may reasonably assume that the mixing region will be 'well mixed' since we have no dissipation to drain energy before it can become so, and it can be shown that the mixing region would progress to $\pm 3z_n/4$. The end state in figure 1(*d*) contains density jumps. Such jumps are consistent with so-called 'external mixing', in which density gradients tend to be sharpened (Turner 1973) by a supply of turbulent energy from a source some distance away. The sharpened density gradient appears in the corresponding p.d.f. as a trough, where densities initially located between $z_n/2$ and $3z_n/4$ are subsumed into the mixing zone. Since baroclinic deposition of vorticity into the flow at precisely the orientation and location required to best enhance scalar gradients is indicative of 'internal mixing', where density contrasts are smoothed rather than sharpened by the turbulent processes, we view figure 1(*d*) as a hypothetical, rather than a realistic, possibility. We also note (Fernando 1991) that the process of external mixing is known to be very inefficient compared with that of Rayleigh–Taylor instability.

However, it is clear that with our new configuration we can obtain statically stable, quiescent end states for the complete range of possible mixing efficiencies. This is not possible with classical Rayleigh–Taylor instability, and indeed all other unstable profiles of the form (1.11), because there the system starts with more available potential energy than is needed to mix completely to a homogeneous end state. Any energy not used in mixing must be dissipated, reducing the average value of η_A

between initial and final states. It appears that the upper limit in the classical case is $\eta_A = 1/2$ simply because of the geometric constraint that the end state must be at least neutrally stable. Previously, this equi-distribution of irreversible energy fluxes between internal energy and background potential energy has been regarded as an intrinsic upper limit of the fluid. However, attributing special significance to this observation is inappropriate, since in the classical Rayleigh–Taylor system one cannot discriminate on the basis of quiescent initial and final states between, on the one hand, that portion of the dissipated energy that was intrinsically required as part of the mixing process to bring fluid parcels of contrasting densities close together so molecular diffusion could take place, and, on the other, that portion that was dissipated due to supplementary advection without having made a significant contribution to mixing.

Equally, in our new configuration, there is no special significance to a particular value of mixing efficiency without reference to the corresponding well-mixed end state; it would be possible to conceive of other initial stratifications whose upper limit of mixing efficiency on the basis of internal mixing was greater than 3/4. The crucial feature of our configuration is that there is much less initially available potential energy than classical Rayleigh–Taylor instability. Provided the mixing efficiency turns out to be lower than the geometric limit, the end state is solely and robustly determined by energy conversions intrinsic to the Rayleigh–Taylor driven mixing mechanism that we regard as being optimal. The following sections describe a series of experiments designed to test and understand these predictions.

2. Experimental setup

The experimental arrangements for the present set of experiments with linearly stratified upper and lower layers follow broadly those for studying classical Rayleigh–Taylor instability. Density differences are created by adding NaCl to fresh water and the basic apparatus is identical to that used by Dalziel *et al.* (1999) and Jacobs & Dalziel (2005), which in turn was refined from earlier studies (Dalziel 1993; Linden *et al.* 1994). The Rayleigh–Taylor tank has dimensions 0.4 m × 0.2 m × 0.5 m as shown in figure 2(*a*), and its central feature is the sliding barrier, which supports the unstable density discontinuity prior to release.

Lane-Serff (1989) conceived of a composite barrier mechanism as detailed in figure 2(*b–d*) made with a structural core of two metal plates, and flexible external surfaces of polyester cloth. The cloth is attached to the tank at one end, and during withdrawal of the barrier at the start of an experiment, the cloth is folded inside the barrier between the metal plates. This shields the fluid from the moving metal, and in the reference frame of the tank the cloth is stationary, except at the very tip of the barrier where it folds around, and a clearance along the edges. The total barrier thickness is 2.5 mm.

Some light-induced fluorescence (LIF) measurements were made in the present study using a 700 W xenon arc lamp, di-sodium fluorescein dye and a 1 Mpixel UNIQVision 1830-12B-CL monochrome charge-coupled device (CCD) digital video camera. Fluid below the unstable density discontinuity was dyed with a uniform concentration of dye, and a very thin (<1 mm) vertical light sheet used. The observations are shown later in § 3. Unlike Rayleigh–Taylor in its classical configuration, here the dye is no longer a proxy for density, and these images instead measure the penetration of the dye front into the undyed upper region.

Quantitative optical measurements were made using a dye attenuation technique. A fluorescent light bank with an optical diffuser (functioning also as a heat shield) was placed behind the tank and recorded by the video camera at a distance of 5 m

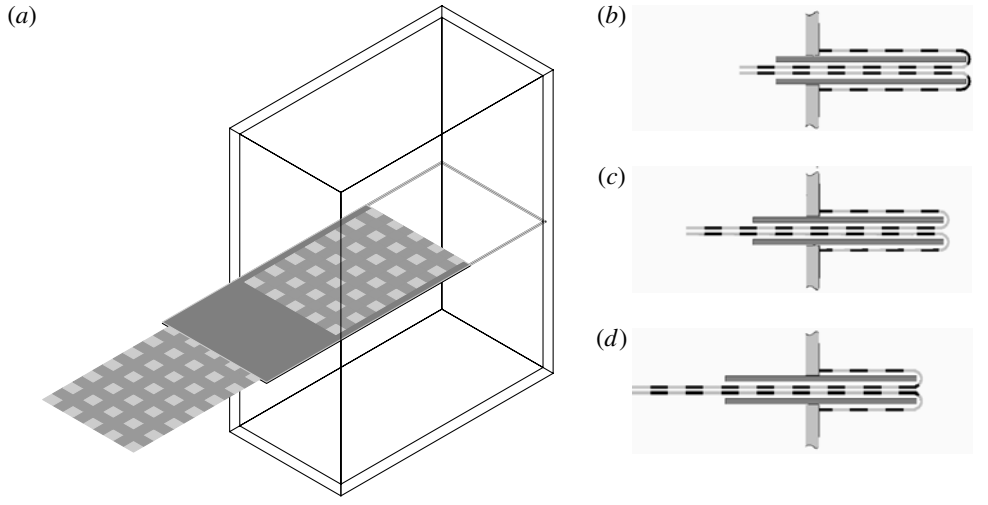

FIGURE 2. Diagrams illustrating tank and barrier mechanism: (*a*) an overview of the tank, with nylon cloth (chequered pattern) and metal barrier (grey); (*b–d*) series of cross-sections of the composite barrier while being withdrawn.

from the front to minimize parallax. Fiesta Red food colouring dye was used, and a green filter was placed over the lens of the camera so that the light transmitted to the CCD sensor was spectrally narrow-band. Recorded images were corrected for variations in background light intensity and calibrated against a known linear dye/density stratification. Attenuation experiments (see Cenedese & Dalziel 1998, for more detail) were performed both where dye was a proxy for density (optical density method) and, like the qualitative observations in figure 3, where dye concentration is uniform within a layer (dye penetration method).

The main focus of this work, however, is calculation of mixing efficiency by accurately measuring the density field. This was performed in a set of experiments using only brine (Schmidt number $Sc = \nu/\kappa = 700$) and without dye. The vertical profile of salt concentration was measured by traversing a conductivity probe. The probe used is an aspirating design, whereby brine is sucked through the 0.3 mm diameter nozzle at very low volume flow rate (10 ml min^{-1}), but this gives a tip velocity of 23 m s^{-1}. The electrical pathway from outer to inner electrode is through the nozzle, and the signal is dominated by the conductivity of fluid in the nozzle. Owing to its high nozzle velocity, the probe has a very fast frequency response. In these experiments the probe was traversed vertically down through the tank at 2 cm s^{-1} using a computer-controlled stepper motor, and voltage measurements from the probe were streamed synchronously to an analogue data acquisition card. Probe measurements were made in quiescent flow (except perhaps for the potential flow response of the probe itself) before and after the system had relaxed.

A pair of computer-controlled peristaltic pumps are used to reliably create the linear stratifications. We note that a temporally nonlinear density variation is required in the supply of fluid to the tank, since mixing between adjacent horizontal layers is influenced by the boundary towards the end of the filling process. Filling was performed with the barrier nearly closed, to minimize the disturbance to the lower layer stratification when closing the barrier to prepare for filling the upper layer. Both layers are initially over-filled by 2 cm to ensure the conductivity probe has an electrical pathway between its electrodes when measuring the very top of each layer.

In the case of the lower layer, the excess fluid above the barrier is removed after the probe measurements have been taken and the barrier has been closed, but before the upper layer fluid is added.

The removal of the barrier as the experiment begins causes a small drop in the potential energy present in the fluid, since the newly created space is filled by upper layer fluid descending 2.5 mm to occupy the volume. However, to leading order, the barrier withdrawal is energetically neutral, since the work done by the fluid on the barrier is equal to this potential energy change. Naturally, when measuring the initial condition for the upper layer, we do so with the barrier shut, so we make an adjustment to the height of initial condition measurements in the upper layer to calculate the equivalent energetic state with the barrier fully withdrawn.

3. Results and modelling

LIF experiments were conducted with a uniform concentration of fluorescent dye in the upper layer and, from the images in figure 3, it is immediately apparent that the height to which the Rayleigh–Taylor instability reaches is constrained by the stratification. Moreover, the dye shows that the mixing region does not reach the neutral buoyancy height z_n, here set to be the top (and bottom) of the tank. This height would only be reached if parcels of fluid immediately below (above) undergo no mixing. Thus molecular mixing influences the height to which upper layer fluid can penetrate the lower layer (and vice versa), as anticipated in our figure 1.

This raises the question of how accurate a predictor of mixing efficiency dye penetration measurements might be and, conversely, whether for a known mixing efficiency the dye penetration could be calculated. If we consider a parameter θ, in the range $0 < \theta \leqslant 1$, representing the penetration height as a fraction of z_n, and we generalize our earlier assumptions to admit an end state with a constant stratification gradient $\gamma = \beta[1 - 1/(2\theta)]$, say, in the mixed region, then we can establish a mixing efficiency in terms of θ. The generalized end-state potential energies are

$$E_{tp}^{\infty} = \int_{-z_n}^{-\theta z_n} (\rho_l - \beta z)\, gz \,\mathrm{d}z + \int_{-\theta z_n}^{\theta z_n} \left(\frac{\rho_u + \rho_l}{2} - \gamma z \right) gz \,\mathrm{d}z + \int_{\theta z_n}^{z_n} (\rho_u - \beta z)\, gz \,\mathrm{d}z$$

$$= -\frac{1+\theta^2}{6} (\rho_u - \rho_l)\, g z_n^2, \tag{3.1a}$$

$$E_{bp}^{\infty} = E_{tp}^{\infty}, \tag{3.1b}$$

and from this we recover the aggregate mixing efficiency as

$$\eta_A = 1 - \theta^2 = 1 - \frac{1}{4(1 - \gamma/\beta)^2}, \tag{3.2}$$

for a non-zero initial stratification gradient β. For energetic consistency (i.e. zero available energy in the final state), $\theta \geqslant 1/2$ since only statically stable density profiles are viable quiescent end states. One feature that becomes obvious from (3.2) is that, with smaller mixing efficiencies, the penetration height θz_n increases. In the immiscible limit, $\theta = 1$. Still larger values of θ are dynamically inadmissible (buoyancy opposes $\theta > 1$), but it is interesting to note that such density profiles have an even lower total potential energy, i.e. E_{tp}^{∞} reduces monotonically with increasing θ. This observation is crucial. It is now evident that penetration into the range $1/2 < \theta < 1$ must release *more* of the initially available potential energy. Incidentally, a larger proportion of this energy must eventually go into dissipation to be consistent

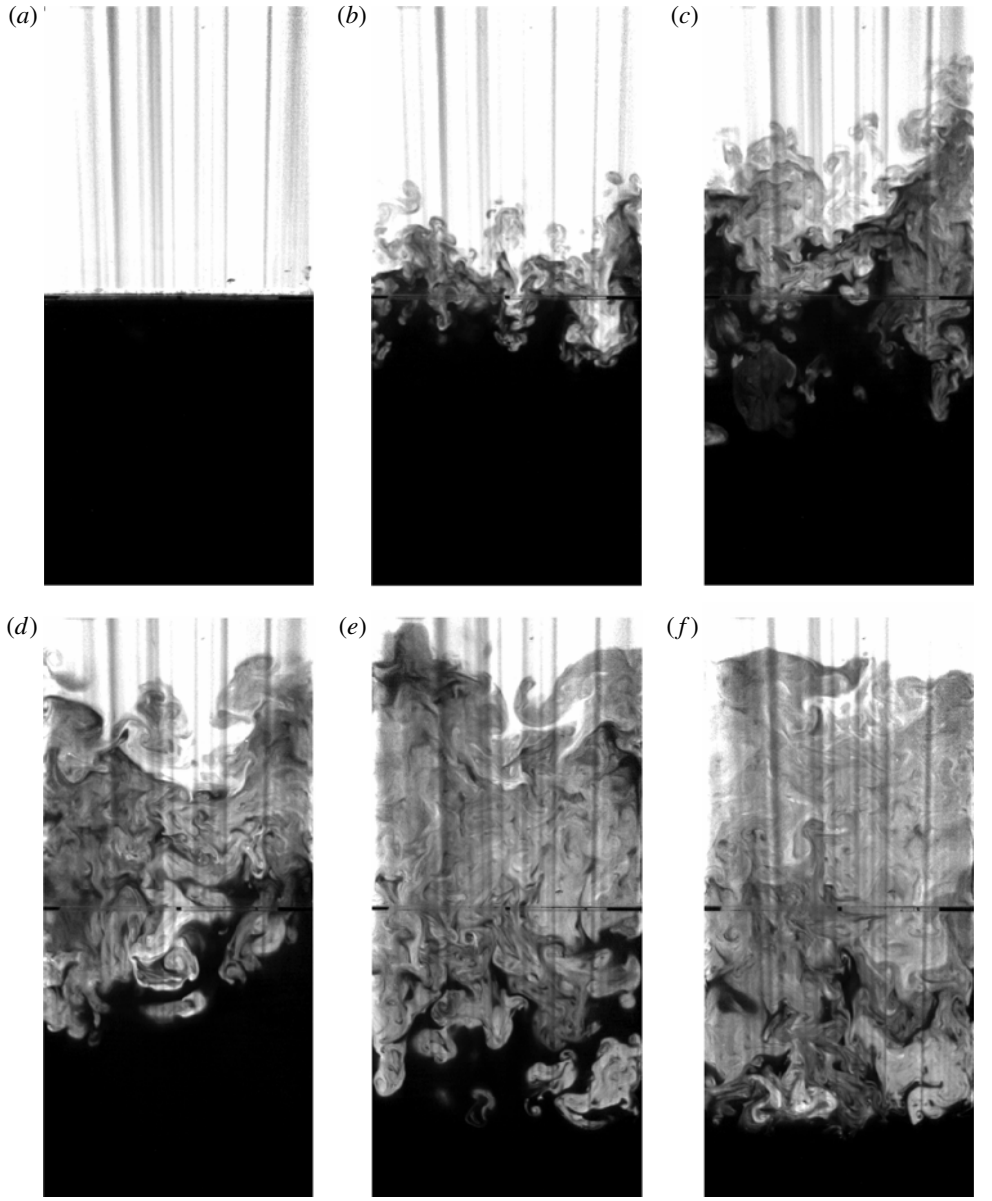

FIGURE 3. Experimental image sequence showing the Rayleigh–Taylor instability confined by linear stratification, at times: (*a*) $t = 0$ s, (*b*) $t = 4$ s, (*c*) $t = 8$ s, (*d*) $t = 12$ s, (*e*) $t = 16$ s and (*f*) $t = 20$ s. The images are captured from the end of the tank, with the barrier withdrawn into the page. The Atwood number is $A = 2 \times 10^{-3}$.

with (3.2). However, it is not apparent from the one-dimensional profile of density how this potential energy can be accessed, since when $\theta > 1/2$ the mean stratification is stable and one might conclude that $E_{ap} = 0$, and any remaining E_a is merely residual kinetic energy that will decay rapidly away. This is not consistent with substantial development of the penetration height beyond $\theta = 1/2$ as observed in the experiments. Our explanation is that, while the horizontally averaged density profile can be used to calculate E_{tp} without error, it only represents a lower bound on E_{ap}, since inclined

isopycnals store additional E_{ap} without appearing in the average. We might write

$$E^t_{tp} - E^t_{bp} < E^t_{ap} < E^t_{tp} - E^0_{bp}, \tag{3.3}$$

since we can construct an upper bound from the 'zero-mixing' limit (where $E_{bp} = \text{const.}$). With this understanding, it is clear that $\theta = 1/2$ is not a limit on the available energy; the absolute limit is determined by the rise in E_{bp}, which is entirely a function of molecular mixing.

It is instructive at this point to reconsider the p.d.f., its relationship to E_{bp} and the inclined isopycnals. In general, the wider the spread of the p.d.f., the lower the background potential energy and the steeper the density gradients of those inclined isopycnals. However, only the portion of the p.d.f. contributed by the mixing region, p.d.f.$|_{mix}$, say, plays a role in the evolution of the flow. For the mixing region to continue growing while the mean density stratification is stable requires the spread of p.d.f.$|_{mix}$ to be greater than the difference between densities at the upper and lower edges of the mixing region. Thus, locally, the flow is Rayleigh–Taylor unstable and fresh fluid above and below the mixing region can be drawn in. It is thermodynamically inadmissible for the p.d.f.$|_{mix}$ to increase its spread with time (this implies un-mixing at a molecular level), so at the time where the mixing zone stops growing, the density spread must be $[\rho_u - \beta\theta z_n, \rho_l + \beta\theta z_n]$. Thereafter, the remaining available energy stored by inclined isopycnals is expended by mixing out these density gradients, p.d.f.$|_{mix}$ clusters towards the mean density and the isopycnals become horizontal. At this point the flow has no further available energy and becomes quiescent. The E_{ap} remaining once θz_n has been reached is merely residual energy, and plays no significant role in modifying the mean density profile. If this were a significant reservoir of available energy, then it would sharpen the density gradients at the edge of the mixing region. While we cannot rule out the possibility at $h > z_n/2$ that there are regions of local static stability in which residual kinetic energy drives some mixing, there is no evidence in figure 3 of the scouring normally associated with such processes. Indeed, subsequent figures will show that, with the present initial stratification, at no point during the evolution of the instability is there evidence of a contribution from mixing of this type to the stratification; rather, there exist localized regions of instability throughout the vertical extent of the mixing region for the duration of the evolution.

We would expect the maximum penetration of dye to be associated with the height $\pm\theta z_n$ of the end-state mixed region. While internal gravity waves are bound to form where the mixing zone interfaces with fluid above and below, in our closed domain energy cannot be radiated away by these waves. Except if they were to break (which we regard as unlikely), they simply exchange E_{ap} with E_k and contribute to the reversible flux $\phi(t)$. We initially (Lawrie 2009) used time-series data from dye penetration LIF and a simple concentration thresholding to define the boundary of the mixed region. While we observed with this measure that the instability settles to a constant height, the ensemble average appeared to overshoot the end-state value during transient growth by 10 %. This was not, however, an observation unique to the LIF viewing plane. Shadowgraph measurements highlight the extrema of turbulent mixing zones rather than a mean or projected view; our measurements covered the whole width and thickness of the tank yet also exhibited a similar overshoot. We attribute the appearance of additional transient penetration to these internal gravity waves, but we expect them to play no significant role in irreversible energy conversion. The experiments presented in this paper use improved diagnostics to focus solely on these irreversible conversions.

To refine our expectations of the form that the transient growth behaviour should take in the new, stratified case, we now examine the exchange between kinetic and potential energies as the Rayleigh–Taylor instability relaxes. The energy budget can be written as

$$\int \overline{\overline{\rho_0}} g z \, \mathrm{d}z - \int \overline{\overline{\rho}} g z \, \mathrm{d}z \sim \int \frac{1}{2} \overline{\overline{\rho \boldsymbol{u}^2}} \, \mathrm{d}z, \tag{3.4}$$

where the double overbar indicates a horizontally averaged quantity, $\overline{\overline{\rho_0}} = \rho(z, 0)$, $\overline{\overline{\rho}} = \rho(z, t)$, and the term $\overline{\overline{\rho \boldsymbol{u}^2}}$ represents kinetic energy. The $\sim$ symbol becomes an equality in the case of no dissipation ($\eta_I = 1$) but in general we expect η_I to be a constant of proportionality. We progress by assuming a functional form for the density perturbation function $\rho'(z, t) = \overline{\overline{\rho_0}} - \overline{\overline{\rho}}$, and evaluating directly. In the first instance we assume that as the system relaxes it forms a well-mixed region of uniform density $(\rho_u + \rho_l)/2$. Thus

$$\begin{aligned} \int_{-z_n}^{z_n} \left(\overline{\overline{\rho_0}} - \overline{\overline{\rho}}\right) g z \, \mathrm{d}z &\sim \int_0^h \left(\frac{\rho_u - \rho_l}{2} - \beta z\right) g z \, \mathrm{d}z + \int_{-h}^0 - \left(\frac{\rho_u - \rho_l}{2} - \beta z\right) g z \, \mathrm{d}z \\ &\sim \frac{1}{2} g h^2 \left(\rho_u - \rho_l\right) \left(1 - \frac{h}{\chi z_n}\right), \end{aligned} \tag{3.5}$$

where $\chi = 3/4$. Following the scalings proposed by Batchelor (1954) and reviewed by Turner (1986) for studies of turbulent entrainment, and in line with previous studies on the self-similar Rayleigh–Taylor instability, we assume that turbulent velocities scale as $\boldsymbol{u} \sim \mathrm{d}h/\mathrm{d}t$. The kinetic energy, after making the Boussinesq approximation, becomes

$$\int_{-z_n}^{z_n} \frac{1}{2} \overline{\overline{\rho \left|\boldsymbol{u}^2\right|}} \, \mathrm{d}z \sim \frac{\rho_u + \rho_l}{2} \left(\frac{\mathrm{d}h}{\mathrm{d}t}\right)^2 \overline{\overline{h}}. \tag{3.6}$$

This energy is distributed over the mixing zone volume, the height of which scales with $\overline{\overline{h}}$, so the energy balance is therefore

$$\frac{1}{2} g h^2 \left(\rho_u - \rho_l\right) \left(1 - \frac{h}{\chi z_n}\right) \sim \frac{\rho_u + \rho_l}{2} \left(\frac{\mathrm{d}h}{\mathrm{d}t}\right)^2 h. \tag{3.7}$$

Defining the buoyancy frequency N for the undisturbed stratification as given in (1.4), the integration to recover $h(t)$ is of the form

$$\int \mathrm{d}t \sim \int \frac{1}{\sqrt{\frac{1}{2} N^2 h z_n [1 - h/(\chi z_n)]}} \frac{\mathrm{d}h}{\mathrm{d}t} \mathrm{d}t, \tag{3.8}$$

to which there is a solution

$$t - t_0 \sim \frac{\sqrt{2\chi}}{N} \arctan\left(\frac{\sqrt{\frac{1}{8}\chi} \, z_n [2h/(\chi z_n) - 1]}{\sqrt{\frac{1}{2} z_n h [1 - h/(\chi z_n)]}}\right). \tag{3.9}$$

This functional form, plotted in figure 5, confirms that we should observe monotonic transient growth of the instability. It is also clear that there is only one single time scale in the problem,

$$\frac{1}{N} = \sqrt{\frac{z_n}{2Ag}}, \tag{3.10}$$

which determines both the Rayleigh–Taylor acceleration and the subsequent deceleration as available energy is consumed. This is also the time scale of any internal gravity waves in the unmixed regions. We can define a Reynolds number for the mixing zone growth as $Re = h(\mathrm{d}h/\mathrm{d}t)/\nu$ and from (3.9) it follows that

$$Re \sim \frac{N z_n^2 \chi^{3/2}}{\nu} \sqrt{\left(\frac{h}{\chi z_n}\right)^3 \left(1 - \frac{h}{\chi z_n}\right)}. \tag{3.11}$$

Clearly spatial and temporal scalings are independent here, so $Re(h)$ is self-similar for all Atwood numbers and, from (3.10), it follows that $Re \sim A^{1/2}$. The most significant features of $Re(h)$, as shown in figure 4, are its asymmetry, with a late peak at $3\chi z_n/4$, and an extremely rapid decay to 0 as $h \to \chi z_n$. Recalling that $\chi = 3/4$, we have a prediction of end-state penetration $h(\infty) = 3z_n/4$ that is consistent with the assumptions in the model, namely that all initially available potential energy is converted to kinetic energy, and all kinetic energy is returned to potential energy, but none is lost through dissipation. This is the $\eta_A = 1$ scenario depicted in figure 1(*d*). Since we know that only a proportion of the kinetic energy is returned to potential energy, given by an instantaneous mixing efficiency η_I, we can begin to reconcile the model prediction with our intuition. To be consistent, we must relax the assumption of well-mixedness and admit other possible end-state gradients. It turns out that this is possible by a simple transformation. For the well-mixed case, the density deficit function $(\overline{\rho_0} - \overline{\rho})$ given in (3.5) has a constant gradient β in the range $z = [-h, h]$, with a discontinuity at $z = 0$. Suppose our end state has a stable slope $-\partial\rho/\partial z = \gamma > 0$, then the corresponding gradient in (3.5) becomes $\beta + \gamma$. Tracking this through the model, we see that this simply changes the coefficient χ, and therefore the predicted end-state penetration $h(\infty)$ is consistent with (3.2). While there are limitations to this modified model (the $\beta + \gamma$ slope of stratification is a poor approximation at early time, for instance), we nevertheless obtain useful insight from the scalings.

An important characterization of buoyant mixing flows in general is the Richardson number. Here, we take a self-consistent definition for the bulk Richardson number based on the density difference $\Delta\rho(h)$ between points just above $(\rho_u - \beta h)$ and just below $(\rho_l + \beta h)$ the mixing region,

$$Ri = g\frac{\Delta\rho(h)}{2\overline{\rho}}\frac{h}{(\mathrm{d}h/\mathrm{d}t)^2} \sim \frac{2h/z_n - 1}{1 - h/(\chi z_n)}. \tag{3.12}$$

It is clear from the functional form, also shown in figure 4, that Ri is negative initially, owing to the unstable mean density gradient within the mixing zone. As h passes through $z_n/2$, the horizontally averaged stratification becomes stable in the mixing zone and $Ri = 0$. As Re begins its rapid decay towards $h/(\chi z_n) = 1$, the flow becomes increasingly stable as Ri grows rapidly. In figure 4 we have plotted Ri for $\chi = 3/4$, consistent with the assumptions in the model. As χ varies, so too will the relative positions of Re_{peak} and $Ri = 0$. However, the kinetic energy $(\mathrm{d}h/\mathrm{d}t)^2$ always peaks at $h/(\chi z_n) = 0.5$, which implies that kinetic energy begins to fall long before the mean stratification is stable, and despite the continued increase in Reynolds number. We note once again that the mean density profile hides available potential energy contained in horizontal density gradients, and so this bulk Richardson number cannot inform us of precisely when mixing turns off. In the case of internal mixing, this is solely determined by the p.d.f. of the density field. Taken together, however, these scalings give an important justification that the system relaxation is dominated by energetic,

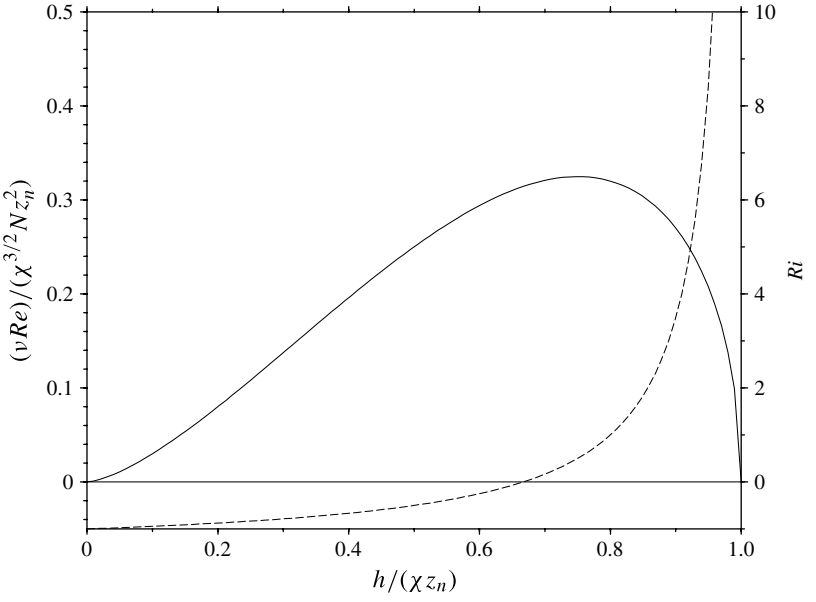

FIGURE 4. Normalized *Re* (solid line) and *Ri* (dashed line) as a function of normalized height.

high-*Re*, low-*Ri* Rayleigh–Taylor mixing and the low-*Re*, high-*Ri* decay phase that must exist just before $h = h(\infty)$ is energetically negligible.

The curve given by (3.9) with a suitable χ is shown as a solid line in figure 5, scaled on the time axis (as with most Rayleigh–Taylor models in the literature, we have no way of estimating the growth time scale) to match data from an experiment using the dye penetration method described in § 2. The most direct experimental analogue of the dye penetration height $h(t)$ given by our model (3.9) would be to select an isosurface of dye concentration. To avoid making an arbitrary choice and improve the robustness of the measurements, we instead follow Dalziel *et al.* (1999) and use an equivalent integral measure of mixing zone height,

$$h_{exp} \sim \int \overline{\overline{c}}(1 - \overline{\overline{c}})\,\mathrm{d}z, \tag{3.13}$$

where $\overline{\overline{c}}(z)$ is the horizontal mean dye concentration, averaged along each light ray and arithmetically across the tank width. A prefactor ensures that the measures $h(\infty)$ and $h_{exp}(\infty)$ are consistent, and provided the concentration profile in the mixing zone is self-similar, they are equivalent for all t. If the dyed layer is $\overline{\overline{c}} = 1$ initially, the integrand is bounded between $0 < \overline{\overline{c}}(1 - \overline{\overline{c}}) < 0.25$, since this function has a maximum when $\overline{\overline{c}} = 0.5$ in the instance of completely mixed upper and lower layer fluid.

The penetration height observed in the experiment corresponds to a mixing efficiency of $\eta = 0.55$; in this and subsequent figures, the dashed line represents the values for $\eta = 0.5$ (the maximum possible in the classical configuration) and the dotted line for $\eta = 0.75$ (the well-mixed limit for internal mixing in the present configuration). It is clear from the obvious consistency with our energy budget model that, unlike the earlier measurements of Lawrie (2009), there is no significant overshoot in the transient growth observed using this more careful definition of h. Once the stable state has been reached, there is an apparent trend of decreasing penetration, but this

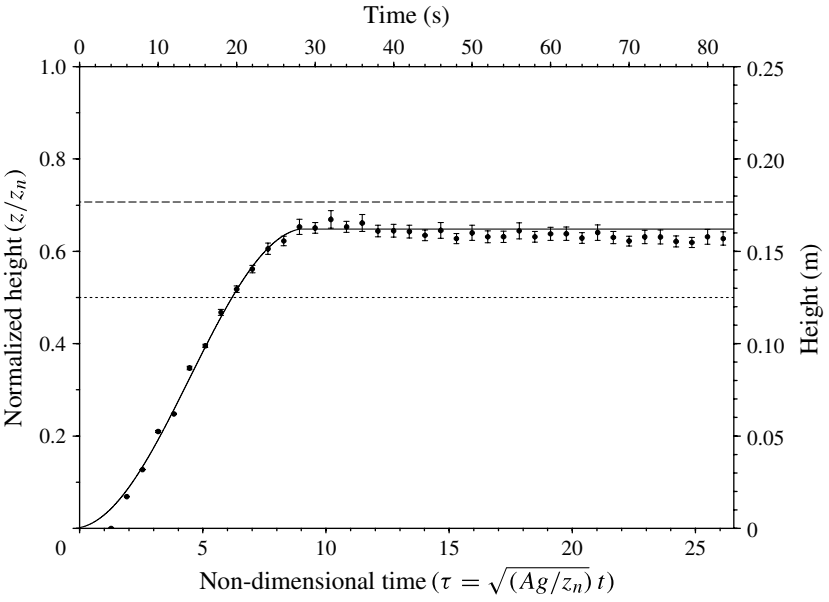

FIGURE 5. Extent of dye interpenetration; optical measurements with model superimposed; $A = 10^{-3}$.

is an artefact of image processing because the fluorescent light bank became slowly brighter during the experiment, not a spuriously non-monotonic development of the instability. The heat emitted by the light bank precluded it being left to equilibrate before starting the experiment, since the red dye absorbs heat and the double-diffusive convection that results interferes with the initial density stratification. The error bars on the experimental data indicate the severity of the correction made to enforce optical conservation of mass, and this accounts for errors due to non-uniformity of density along each light ray.

We also used the dye attenuation technique in 'optical density' mode to obtain a more detailed picture of the density field during the transient growth. Figure 6 shows a sequence of vertical mean profiles $\overline{\overline{\rho}}(z)$. As one would expect, the mixing due to the instability reduces the severity of the density gradient around the Rayleigh–Taylor unstable interface. During the time that the mean density gradient remains unstable, it is obvious how the potential energy is supplied to the system; this becomes less clear when $\partial\overline{\overline{\rho}}/\partial z < 0$ everywhere. Our justification is that the turbulent motion produces horizontal as well as vertical density fluctuations, and therefore statically stable mean stratifications can hide available energy, which will continue to be used for mixing. Thus, locally, the flow is still Rayleigh–Taylor unstable, and able to draw new fluid into the mixing region. In doing so, the mean stratification $\partial\overline{\overline{\rho}}/\partial z$ becomes more stable and, somewhat counter-intuitively, the total potential energy of the system reduces. This continued release of potential energy allows the mean vertical profile to evolve long after the slope in the central mixing region reaches $\partial\overline{\overline{\rho}}/\partial z = 0$. This is not simply residual decay of motion from previously supplied potential energy, but is driven by newly released energy made available by the increasing static stability of the mean profile. In this manner, potential energy could be extracted from the system indefinitely if buoyancy were not opposing further progress of the mixing region. The buoyancy in the system is regulated by the mixing occurring as the system relaxes, and this

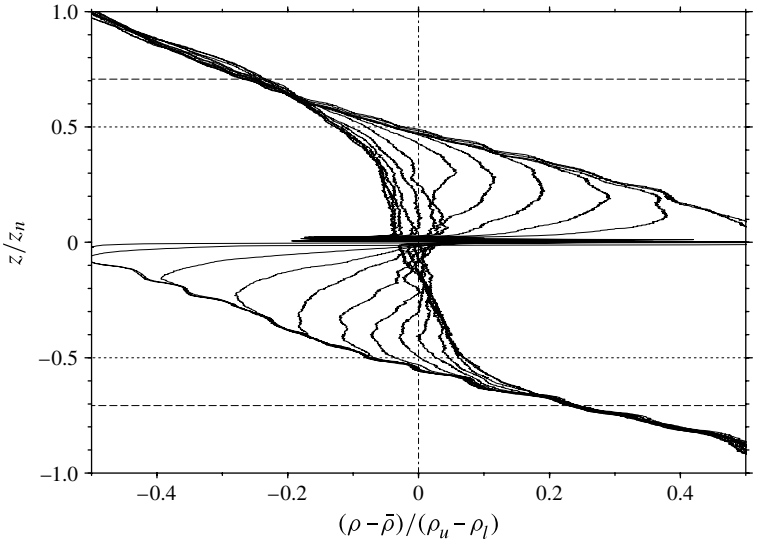

FIGURE 6. Optical measurements of density profile with time $0 < t < 12.5s$, at intervals of 2 s; $A = 10^{-3}$.

determines p.d.f.$|_{mix}$. In turn, this also determines the availability of potential energy in the system. So we therefore arrive at the central conjecture of this paper, that in the present configuration the fluid is free to select a stable state unconstrained by geometric limits, and this stable state unambiguously describes the balance of irreversible energy conversions taking place in Rayleigh–Taylor driven mixing.

The estimated peak Re given by (3.11) for these $A = 10^{-3}$ experiments is $Re_{peak} = 2100$ but, from examination of figure 3, we caution that the integral scale of the turbulence is significantly smaller than the size of the layer, though we believe that the velocities at this length scale are similar to $\mathrm{d}h/\mathrm{d}t$. Having developed an understanding of the fluid mechanical processes in the problem using optical techniques at these very low Atwood numbers, we considered a range of Atwood numbers in the Boussinesq regime, $0.001 < A < 0.012$. As the interfacial density jump increases, $Re(h) \sim A^{1/2}$, but $Ri(h)$ is unchanged. The higher Re regime is interesting since we might anticipate that, as the Kolmogorov scale reduces, mixing efficiency improves. Unfortunately, at higher salt concentrations the refractive index differences between the extreme densities ρ_u and ρ_l are non-negligible, so we solely used beginning- and end-state data from vertical traversals of the conductivity probe.

Figure 7 shows these measurements, normalized by the interfacial density difference and corrected to enforce conservation of mass between beginning and end states in each case. The collapse is good, particularly with respect to stratification slope at $z = 0$ and the inferred penetration height θz_n. From our earlier modelling we would therefore expect the mixing efficiency to be consistent across the Atwood/Reynolds number range. We confirmed this, as shown in figure 8, by direct integration of the potential energies associated with the probe density profiles (black squares with error bars), and compared these to predictions from our simple model (circles), which assumes the stratification is piecewise linear with a mixing zone slope based on $(\mathrm{d}\rho/\mathrm{d}z)|_{z=0}$. In the low Atwood number case we were able to verify mean profiles from optical measurements (triangle) against the probe data.

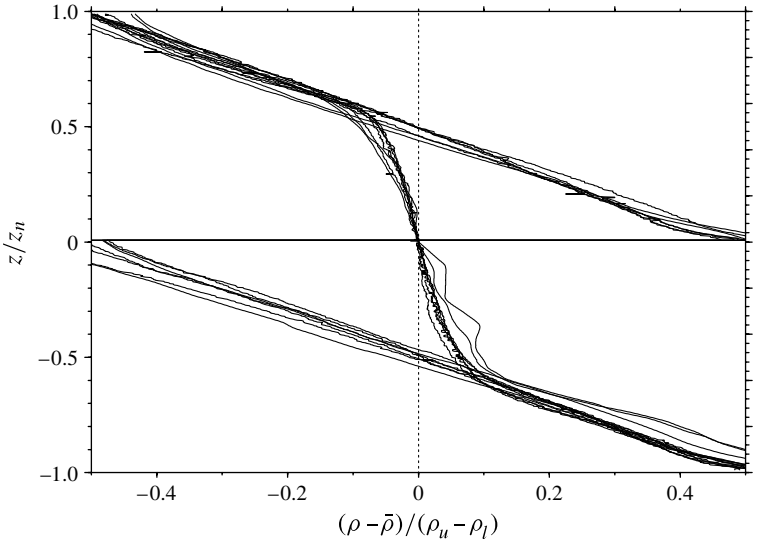

FIGURE 7. Collapse of stratification gradient over the range $0.001 < A < 0.012$, normalized by interfacial density difference.

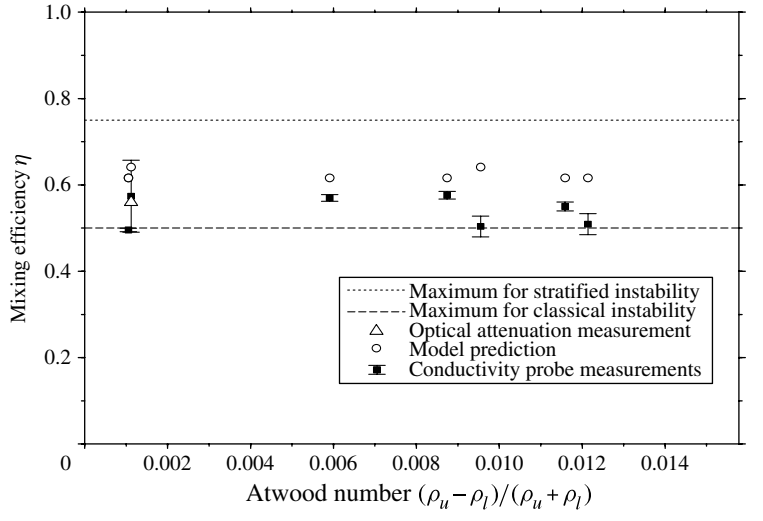

FIGURE 8. Mixing efficiency as a function of Atwood number.

The error bars given for the probe data indicate the uncertainty in experimental mass conservation. A complex arrangement of seals ensured that leakage from the tank through the slot for the barrier was negligible. The small variations in mass we measured between start and end states simply arise from measurement errors in the probe data, partly due to contamination of the probe by silicone grease used to help seal the barrier. The particularly large error range in one $A = 0.001$ case arises from electrical noise in the traverse mechanism influencing the conductivity signal; the signal-to-noise ratio at low salt concentrations is poor, and the outlying data in figure 7 are from the two $A = 0.001$ cases.

The barrier is withdrawn by hand, and a small and inevitably inconsistent contribution to the initial kinetic energy must therefore result. While such variations are unavoidable in our experiment, we believe that they have a comparatively small effect on the mixing efficiency. The conductivity probe data (black squares with error bars) shown in figure 8 account for a 'mean withdrawal', using estimates for the barrier kinetic energy derived in Dalziel *et al.* (1999) from particle tracking velocimetry in a uniform-density Rayleigh–Taylor-neutral fluid ($\rho_u = \rho_l,\ \beta = 0$). The correction results in a 1 % reduction in our calculated values, though we note that this does not account for any long-lasting effects on the structure of the Rayleigh–Taylor turbulence caused by the initial kinetic energy. Across the Atwood number range, experiments with similar initial Atwood numbers appear to give either a mixing efficiency close to $\eta = 0.5$ or a larger value ($\eta \approx 0.56$). We do not believe that this indicates that the instability is bimodal; rather we think that this indicates the extent of variability introduced by the initial perturbation, over which we have little control.

Despite some variability between experiments, from figure 7 we see that the end-state stratification slope is approximately constant, hence so too is our model prediction of mixing efficiency (circles in figure 8). The model does not show especially good agreement with the conductivity probe data, but it must be borne in mind that the model assumes that the stratification slope can be approximated as piecewise linear. A higher-order shape function would doubtless improve the agreement over the current model.

Over the range of Atwood and Reynolds numbers considered ($0.001 < A < 0.012,\ \ 2100 < Re_{peak} < 7300$), we have shown that there is approximate invariance of mixing efficiency, and that the value is well below the energetically admissible maximum. This is in marked contrast to experiments – including those using similar equipment and techniques – performed on the Rayleigh–Taylor instability between two homogeneous layers of equal depth, which routinely measure mixing efficiencies close to the admissible maximum (Holford *et al.* 2003).

This classical Rayleigh–Taylor instability is unusually efficient for doing mixing for two reasons. Firstly, as argued in Dalziel *et al.* (2008), the only energetic route that achieves molecular mixing is a conversion of available potential energy to background potential energy, and by construction the available potential energy already exists in Rayleigh–Taylor instability at $t = 0$. Other less efficient processes need prior conversion of kinetic energy to available potential energy before molecular mixing can take place and there are inevitably associated losses. Secondly, over all scales of the turbulence, the steepest scalar gradients and velocity gradients are co-located, whereas, for example, grid-generated turbulence above a stable density interface (see Fernando 1991) is relatively inefficient because much of the turbulent kinetic energy is dissipated before reaching the interface and being able to do mixing.

However efficient the classical Rayleigh–Taylor problem may be, its geometry imposes an upper bound on possible values of aggregate mixing efficiency. We have found a new Rayleigh–Taylor unstable configuration whose geometry imposes no limit on the possible values of mixing efficiency, and therefore we believe that the experimental data in this paper characterize the fluid's natural or intrinsic mixing efficiency.

4. Conclusions

Since the physical mechanisms in Rayleigh–Taylor instability present optimal conditions for the stretching of material surfaces in a fluid, we have sought to characterize the mixing efficiency of the Rayleigh–Taylor process. The classical form

of Rayleigh–Taylor instability in a finite box has an inherent restriction on the values that mixing efficiency can take, and measurements of initial and final density profiles do not solely characterize the Rayleigh–Taylor mixing, but represent an average over a mixing-intensive phase and a dissipation-dominated phase. Here, Rayleigh–Taylor instability has been examined in a novel configuration chosen to avoid such misleading properties, and we have shown that there is a one-to-one relationship between the form of the end-state density profile and the mixing efficiency, and that our configuration has no restriction on the values that mixing efficiency can take.

A sequence of experiments on an incompressible, miscible fluid system with a Rayleigh–Taylor unstable interface situated between two stable linear stratifications has been conducted. The interpenetration of fluids from above and below the Rayleigh–Taylor unstable interface has been measured by taking vertical density profiles with optical techniques and more accurate measurements taken with an aspirating conductivity probe in quiescent flow before and after system relaxation. Simple linear models predict well the transient growth and the maximal extent of upper and lower layer interpenetration, which is also verifiable from LIF and dye attenuation experimental data. To within the limits of experimental error, the results suggest that the mixing efficiency is invariant with Atwood number over a range of Boussinesq density differences. Under half the energy being spent irreversibly leaves the system as heat, and the remaining portion becomes background potential energy due to irreversible structural changes in the p.d.f. of the density profile associated with molecular diffusion of density. This alone is not significant, since we must consider the observed mixing efficiency against the corresponding value for ideal mixing, and this depends on geometry and the form of mixing one expects. In our case, the observed mixing efficiency is significantly below that for ideal *internal* mixing, a lower bound than our geometry permits, and we argue that our data characterize the intrinsic ability of the fluid to mix in Rayleigh–Taylor instability. Since Rayleigh–Taylor instability appears to be an optimal mixing mechanism, we speculate that our measurements characterize an upper bound on fluid mixing in general.

We would like to thank D. Youngs and R. Williams for many useful discussions and AWE Ltd. for financial support on the research fellowship ‘Leveraging Rayleigh–Taylor instability’.

REFERENCES

BATCHELOR, G. K. 1954 Heat convection and buoyancy effects in fluids. *Q. J. R. Meteorol. Soc.* **80**, 339–358.

CABOT, W. H. & COOK, A. W. 2006 Reynolds number effects on Rayleigh–Taylor instability with implications for type 1a supernovae. *Nat. Phys.* **2**, 562–568.

CENEDESE, C. & DALZIEL, S. B. 1998 Concentration and depth fields determined by the light transmitted through a dyed solution. In *Proceedings of the 8th International Symposium on Flow Visualization* (ed. G. M. Carlomango & I. Grant), p. 061.

COOK, A. W., CABOT, W. & MILLER, P. L. 2004 The mixing transition in Rayleigh–Taylor instability. *J. Fluid Mech.* **511**, 333–362.

DALZIEL, S. B. 1993 Rayleigh–Taylor instability: experiments with image analysis. *Dyn. Atmos. Oceans* **20**, 127–153.

DALZIEL, S. B., LINDEN, P. F. & YOUNGS, D. L. 1999 Self-similarity and internal structure of turbulence induced by Rayleigh–Taylor instability. *J. Fluid Mech.* **399**, 1–48.

DALZIEL, S. B., PATTERSON, M. D., CAULFIELD, C. P. & COOMARASWAMY, I. A. 2008 Mixing efficiency in high-aspect-ratio Rayleigh–Taylor experiments. *Phys. Fluids* **20**, 065106.

DIMONTE, G., YOUNGS, D. L., DIMITS, A., WEBER, S., MARINAK, M., WUNCH, S., GARASI, C., ROBINSON, A., ANDREWS, M. J., RAMAPRABHU, P., CALDER, A. C., FRYXELL, B., BIELLO, J., DURSI, L., MACNEICE, P., OLSON, K., RICKER, P., ROSNER, R., TIMMES, F., TUFO, H., YOUNG, Y. N. & ZINGALE, M. 2004 A comparative study of the turbulent Rayleigh–Taylor instability using high-resolution three-dimensional numerical simulations: the Alpha-Group collaboration. *Phys. Fluids* **16**, 1668.

FERNANDO, H. J. S. 1991 Turbulent mixing in stratified fluids. *Annu. Rev. Fluid Mech.* **23**, 455–493.

HOLFORD, J. M., DALZIEL, S. B. & YOUNGS, D. L. 2003 Rayleigh–Taylor instability at a tilted interface in laboratory experiments and numerical simulations. *Laser Part. Beams* **21**, 419–423.

ITSWEIRE, E. C., KOSEFF, J. R., BRIGGS, D. A. & FERZIGER, J. H. 1992 Turbulence in stratified shear flows: implications for interpreting shear-induced mixing in the ocean. *J. Phys. Oceanogr.* **23**, 1508–1522.

JACOBS, J. W. & DALZIEL, S. B. 2005 Rayleigh–Taylor instability in complex stratifications. *J. Fluid Mech.* **542**, 251–279.

LANE-SERFF, G. F. 1989 Heat flow and air movement in buildings. PhD thesis, DAMTP, University of Cambridge, UK.

LAURENT, L. C., SIMMONS, H. L. & JAYNE, S. R. 2006 Estimating tidally driven mixing in the deep ocean. *Geophys. Res. Lett.* **29**, 2106.

LAWRIE, A. G. W. 2009 Rayleigh–Taylor mixing: confinement by stratification and geometry. PhD thesis, DAMTP, University of Cambridge, UK.

LINDEN, P. F., REDONDO, J. M. & YOUNGS, D. L. 1994 Molecular mixing in Rayleigh–Taylor instability. *J. Fluid Mech.* **265**, 97–124.

MUNK, W. & WUNSCH, C. 1998 Abyssal recipes II: energetics of tidal and wind mixing. *Deep-Sea Res. Part I: Ocean. Res. Papers* **45**, 1977–2010.

OAKEY, N. S. 1982 Determination of the rate of dissipation of turbulent energy from simultaneous temperature and velocity shear microstructure measurements. *J. Phys. Oceanogr.* **22**, 256–271.

OFER, D., ALON, U., MCCRORY, D., SHVARTS, R. L & VERDON, C. P. 1996 Modal model for the nonlinear multimode Rayleigh–Taylor instability. *Phys. Plasmas* **3**, 3073.

READ, K. I. 1984 Experimental investigation of turbulent mixing by Rayleigh–Taylor instability. *Physica* D **12**, 45–58.

RIKANATI, A., ORON, D., ALON, U. & SHVARTS, D. 2000 Statistical mechanics merger model for hydrodynamic instabilities. *Astrophys. J. Suppl. Ser.* **127**, 451–457.

SNIDER, D. M. & ANDREWS, M. J. 1994 Rayleigh–Taylor and shear driven mixing with an unstable thermal stratification. *Phys. Fluids* **6**, 3324–3334.

TAILLEUX, R. 2009 On the energetics of stratified turbulent mixing,irreversible thermodynamics, Boussinesq models, and the ocean heat engine controversy. *J. Fluid Mech.* **638**, 339–382.

TSENG, Y. & FERZIGER, J. H. 2001 Mixing and available potential energy in stratified flows. *Phys. Fluids* **13**, 1281–1293.

TURNER, J. S. 1973 *Buoyancy Effects in Fluids*. Cambridge University Press.

TURNER, J. S. 1986 Turbulent entrainment: the development of the entrainment assumption, and its application to geophysical flows. *J. Fluid Mech.* **173**, 431–471.

WADDELL, J. T., NIEDERHAUS, C. E. & JACOBS, J. W. 2001 Experimental study of Rayleigh–Taylor instability: low Atwood number liquid systems with single-mode initial perturbations. *Phys. Fluids* **13**, 1263–1273.

WINTERS, K. B., LOMBARD, P. N., RILEY, J. J. & D'ASARO, E. A 1995 Available potential energy and mixing in density-stratified fluids. *J. Fluid Mech.* **289**, 115–128.

WINTERS, K. B. & YOUNG, W. R. 2009 Available potential energy and buoyancy variance in horizontal convection. *J. Fluid Mech.* **629**, 221–230.

WUNSCH, C. & FERRARI, R. 2004 Vertical mixing, energy and the general circulation of the oceans. *Annu. Rev. Fluid Mech.* **36**, 281–314.

YOUNGS, D. L. 1984 Numerical simulation of turbulent mixing by Rayleigh–Taylor instability. *Physica* D **12**, 32–44.

ZUFIRIA, J. 1988 Bubble competition in Rayleigh–Taylor instability. *Phys. Fluids* **31**, 440–446.